Dynamics of qudit gates and effects of spectator modes on optimal control pulses

A. Barış Özgüler
Fermi National Accelerator Laboratory, Batavia, IL, 60510 and
Superconducting Quantum Materials and Systems Center (SQMS), Fermilab

Joshua A. Job
Lockheed Martin Advanced Technology Center, Sunnyvale, CA, 94089 and
Superconducting Quantum Materials and Systems Center (SQMS), Fermilab

(Dated: July 20, 2022)

Qudit gates for high dimensional quantum computing can be synthesized with high precision using recent numerical quantum optimal control techniques. Large circuits are broken down into modules and the tailored pulses for each module can be used as primitives for a qudit compiler. Application of the pulses of each module in the presence of extra modes may decrease their effectiveness due to crosstalk. In this paper, we address this problem by simulating qudit dynamics for circuit quantum electrodynamics (cQED) systems. As a test case, we take pulses for single-qudit SWAP gates optimized in isolation and then apply them in the presence of spectator modes each of which are in Fock states. We provide an experimentally relevant scaling formula that can be used as a bound on the fidelity decay. Our results show that frequency shift from spectator mode populations has to be $\lesssim 0.1\%$ of the qudit's nonlinearity in order for high-fidelity single-qudit gates to be useful in the presence of occupied spectator modes.

I. INTRODUCTION

With the demonstrations of qudit control in quantum devices, such as trapped ions [1], photonic processors [2], and circuit quantum electrodynamics (cQED) systems [3–7], many computational levels can be successfully manipulated in order to design and execute quantum algorithms [8]. Compared to its qubit counterparts, high dimensional quantum computing has many advantages, some of which are lower-depth circuits, noise improvement with hardware-efficient solutions [8–11] and efficient means for large-scale quantum information experiments to be performed in the lab, such as black hole dynamics modeled as a scrambling unitary [12].

Quantum devices can be controlled optimally via external fields [13–15]. Gates can be designed in modules (1- and 2-qudit gates), such as in Ref. [16] for bosonic modes. To be able to use synthesized gates in the entire space by preserving their fidelity, one needs to check if the modules play well with the entire space. We leverage `Juqbox.jl` to synthesize qudit SWAP gates with B-spline parametrization following the techniques in [17, 18]. SWAP operations provide simple, yet effective demonstrations for the effects of frequency shifts, which alter the ideal transitions between energy levels and cause fidelity decay.

We outline the rest of the paper. In Section II, we provide the effective Hamiltonian of the driven qudit when it interacts with spectator modes each of which are in Fock states. In Section III, the infidelity scaling is given analytically and compared with the numerical result. Finally, in Section IV, we conclude the paper with discussing future work including ways to alleviate the fidelity decay.

II. EFFECTIVE HAMILTONIAN AND FREQUENCY SHIFT IN THE PRESENCE OF SPECTATOR MODES

We focus here on a cQED system with many oscillators/modes. The system Hamiltonian in the rotating frame for each oscillator is given by [13, 14, 18]:

$$H = -\sum_i \frac{\xi_i}{2}(\hat{n}_i\hat{n}_i - \hat{n}_i) - \sum_{j>i}\xi_{ij}\hat{n}_i\hat{n}_j, \qquad (1)$$

where ξ_i is the self-Kerr for each oscillator i, and ξ_{ij} is the cross-Kerr between oscillators i and j. If we take the state at time t to be a product state of the form $|\psi\rangle \otimes \left|\prod_j n_j\right\rangle$, with the state on the target oscillator $|\psi\rangle$ and spectator modes in Fock states $\{n_j\}$, it is easy to see that the action of the system Hamiltonian will be

$$H|\psi\rangle \otimes_j |n_j\rangle = \Big[-\frac{\xi_1}{2}(\hat{n}_1\hat{n}_1 - \hat{n}_1) - \sum_{j>1}\xi_{1j}n_j\hat{n}_1 + C\Big]|\psi\rangle \otimes_j \left|\prod_j n_j\right\rangle \qquad (2)$$

where C is a constant formed by the action of H on the spectator modes which we ignore from here on as it only generates a global phase.

This manuscript has been authored by Fermi Research Alliance, LLC under Contract No. DE-AC02-07CH11359 with the U.S. Department of Energy, Office of Science, Office of High Energy Physics.

The above Hamiltonian does not generate any evolution on the spectator modes (because their initial state is Fock state), and so focusing only on the target mode and suppressing the subscript 1 for ease of notation we get the effective Hamiltonian on the target mode:

$$H_{eff} = -\frac{\xi}{2}(\hat{n}\hat{n} - \hat{n}) - \sum_j \xi_j n_j \hat{n}, \tag{3}$$

where the first term $H_0 \equiv -\frac{\xi}{2}(\hat{n}\hat{n} - \hat{n})$ is the time-independent part of the driven qudit Hamiltonian, $\varepsilon \equiv \sum_j \xi_j n_j$ is the perturbation parameter and $V \equiv -\hat{n}$ is the shift operator appearing due to spectators. In essence, the cross-Kerr between the target mode and the spectator modes in Fock states produces a frequency shift on the target mode. We can write in short:

$$H_{eff} = H_0 + \varepsilon V. \tag{4}$$

III. SCALING OF THE INFIDELITY

For the quantum control problem of gate synthesis, the target action U is known, and we wish to find a time-dependent drive Hamiltonian $H_d(t)$ such that the evolution from $H(t) = H_0 + H_d(t)$ produces the target unitary. The propagator for the driven qudit without spectator modes is given by:

$$U_0(t) = \mathcal{T} \exp\left[-\frac{i}{\hbar}\int_0^t dt' \left(H_0 + H_d(t')\right)\right], \tag{5}$$

where H_d is the drive term synthesizing the target gate, i.e., $U_0(t=\tau)$ is the target gate U, and τ is the gate time. Using the same drive terms, the effective propagator of the qudit due to spectator shifts is given by:

$$U_{eff}(t) = \mathcal{T} \exp\left[-\frac{i}{\hbar}\int_0^t dt' \left(H_{eff} + H_d(t')\right)\right]. \tag{6}$$

Fidelity between the ideal gate and shifted gate is defined as:

$$F(t) \equiv \left|\frac{Tr(U_{rot}(t))}{d}\right|^2, \tag{7}$$

where $U_{rot}(t) \equiv U_0^\dagger(t)\, U_{eff}(t)$ is the propagator in the rotating frame of the driven qudit, d is the norm of $U_0(t)$.

U_{rot} is defined in terms of the perturbation as:

$$U_{rot}(t) = \mathcal{T} \exp\left[-\frac{i}{\hbar}\int_0^t dt' \tilde{V}(t')\right], \tag{8}$$

where $\tilde{V}(t) \equiv U_0^\dagger(t) V U_0(t)$. For small perturbation ε, U_{rot} is expanded via Baker–Campbell–Hausdorff formula as in Ref. [19]:

$$U_{rot}(t) \simeq \exp\left[-\frac{i}{\hbar}\Big(\varepsilon \bar{V} t + \frac{1}{2}\varepsilon^2 \Gamma(t) + \mathcal{O}(\varepsilon^3)\Big)\right], \tag{9}$$

where $\bar{V}$ is the time average of $\tilde{V}(t)$:

$$\bar{V} = \frac{1}{\tau}\int_0^\tau \tilde{V}(t')dt', \tag{10}$$

and $\Gamma(t)$ is the integral of the time correlation function:

$$\Gamma(t) = \frac{i}{\hbar}\int_0^t dt' \int_{t'}^t dt''[\tilde{V}(t'), \tilde{V}(t'')]. \tag{11}$$

$U_{rot}(t)$ is:

$$U_{rot}(t) \simeq \mathbb{I} + X + \frac{X^2}{2} + ..., \tag{12}$$

where $X \equiv -\frac{i}{\hbar}\Big(\varepsilon \bar{V} t + \frac{1}{2}\varepsilon^2 \Gamma(t)\Big)$. Fidelity at $t = \tau$:

$$F(\tau) \simeq 1 - \frac{\Big[Tr(\bar{V}^2) - Tr^2(\bar{V})\Big]\tau^2}{\hbar^2\, d^2}\varepsilon^2. \tag{13}$$

The normalized trace term in the coefficient of ε^2 is known as fidelity susceptibility for time-independent systems [20, 21]. We leave the detailed examination of this trace term with time-averaged operators for future work. We compare this analytical scaling ($\sim \varepsilon^2$) with numerical results below ($cf.$ Fig. 2).

To design a gate using optimal control techniques, we optimize pulse control terms $\hat{a} + \hat{a}^\dagger$ and $\hat{a} - \hat{a}^\dagger$ acting on the target oscillator (thus, they commute with the spectator modes). Transitions between the Fock states $|i\rangle$ and $|j\rangle$ in the oscillator are generated by control pulses at the transition frequency between the states, in our case that is $\frac{\xi}{2}(i^2 - j^2 + i - j)$. The spectator modes, however, shift these frequencies by $\sum_k \xi_k n_k (i - j)$.

To demonstrate the effect of this frequency shift, we can optimize a set of control pulses to produce a swap gate between $|0\rangle$ and $|j\rangle$ on a spectator mode. For concreteness, we use $\omega/2\pi = 4.8$GHz and $\xi/2\pi = 0.22$GHz, with the self-Kerr of the spectator modes being modulated as some fraction of ξ and cross-Kerr parameters equal to $\beta_j \xi$ with parameter β_j varying for each mode j. We use these system parameters so that our gates are directly comparable to those in Section 7 of Ref. [17]. Other parameters, such as which SWAPs will be generated (SWAPs from $|0\rangle$ to $|3\rangle, |4\rangle, |5\rangle, |6\rangle$) and the time for each gate ($140, 215, 265$, and 425 ns respectively) are also

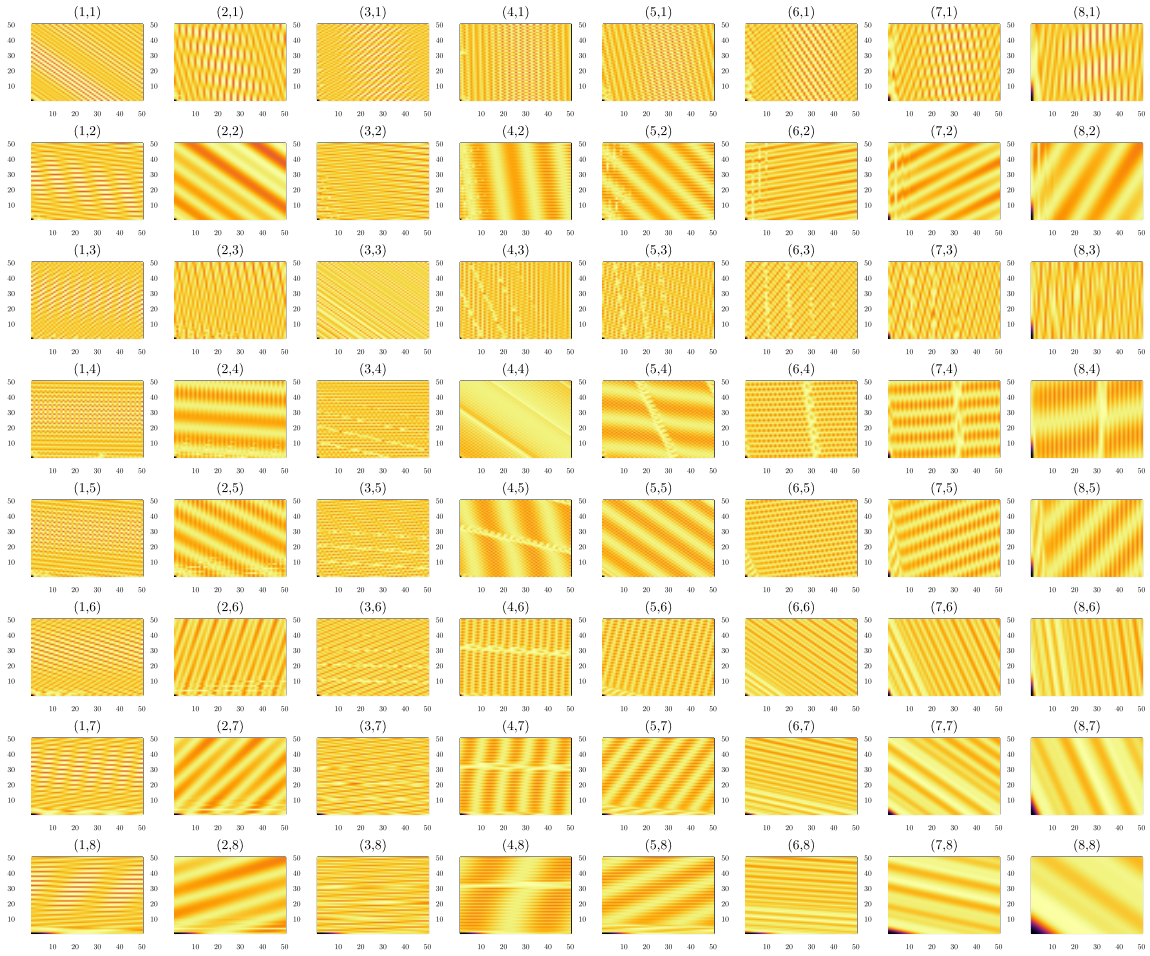

Figure 1: Heatmaps of infidelity (black/purple = 0, ie perfect fidelity, white/yellow = 1) of the $|0\rangle\,|4\rangle$ transition. Each pixel in each heatmap is a given photon occupation of the spectator modes (from 0 to 50 for oscillator 1 (x-axis) and oscillator 2 (y-axis))) with the title of each subplot denoting the cross-Kerr to spectator modes in tuples (i, j), where the cross Kerr to the 1st (2nd) oscillator is set to be $10^{(i-1)/2}\xi$ ($10^{(j-1)/2}\xi$). The top-left heatmap Top-left has a frequency shift of size ξ for each photon in neighboring cavities, while the bottom-right heatmap has a shift of $10^{-3.5}\xi$ per photon in the spectator modes, resulting in a 3.2% shift in frequency for 50 photons in each spectator mode (100 photons total). You can see for off-diagonal terms the oscillatory behavior is very different on each axis corresponding to the differing magnitude of the frequency shifts from cross-Kerr interactions due to spectator mode occupation.

taken from that section, along with the use of a single guard level (which implies that a SWAP to state $|k\rangle$ has $k+1$ levels actively participating in the gate and $k+2$ states simulated in the optimization and frequency-shifted calculations). Our only difference is that we restricted our optimization of the control parameters for the ideal (without spectator modes) case to 200 iterations. Note that our simulations were performed for closed systems but noise is not a bottleneck for this work since pulse durations are much shorter than typical coherence times for cQED systems, such as superconducting cavities [3, 6, 7].

A SWAP gate between level $|i\rangle$ and $|j\rangle$ is defined as:

$$\mathrm{SWAP}_{|i\rangle\leftrightarrow|j\rangle} = \mathbb{I} + |i\rangle\langle j| + |j\rangle\langle i| - |i\rangle\langle i| - |j\rangle\langle j|\,. \quad (14)$$

SWAP gates are vital for shifting matrix elements around and moving quantum states around lattices of qubits, while partial SWAP operations can generate entanglement and more complicated superpositions. Here, our choice of simple SWAPs between the ground state and various excited states of the single oscillator is meant as only an example to illustrate the effect of spectator mode shift of the target oscillator's transition frequencies.

Below, in Fig. 1, we show the fidelity of the im-

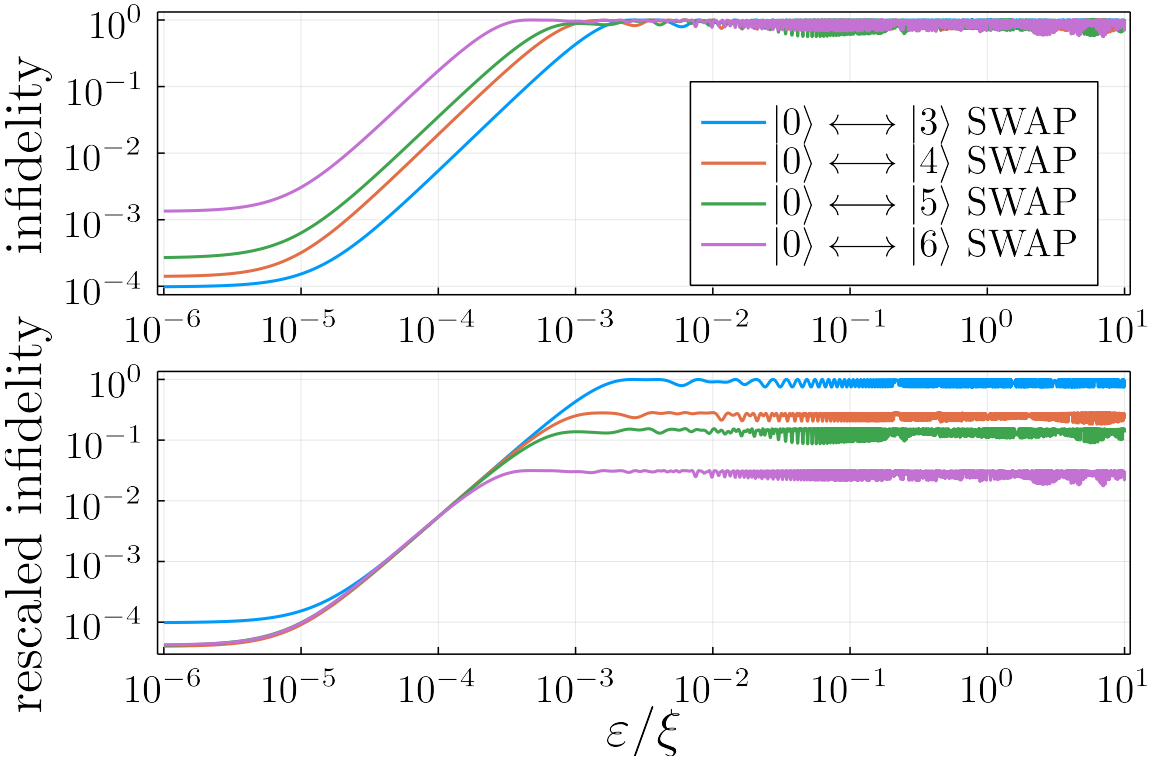

Figure 2: **(Above)** Infidelity for the labeled SWAP operation arising from a frequency shift $\varepsilon = \Sigma_j \xi_j n_j$ from the presence of n_j photons in the jth spectator mode with cross-Kerr strength to the target mode ξ_j. We exclude zero occupation as the x-axis value would be 0, but the infidelity for that ideal case is $\mathcal{O}(10^{-4})$ to $\mathcal{O}(10^{-3})$ for each gate, as seen at the smallest ε. The slope for small $\varepsilon/\xi = \mathcal{O}(10^{-4})$ is ≈ 2, meaning that infidelity scales quadratically with ε. The flat region at very small ε is the region when the perturbation is negligible, while for larger ε higher order terms (in part due to saturation near infidelity ≈ 1) take effect. **(Below)** Rescaled fidelity curves such that the value at the $\varepsilon = 10^{-4}$ for each curve is equal, so as to highlight the similarity of the slope in that region.

plemented gate when we optimize our control pulse taking into account only the Hamiltonian on the target mode, ignoring spectator modes, and then apply those pulses to a system with spectator modes of various cross-Kerr parameters for various occupations in the spectator modes. Specifically, we plot 2D heatmaps for the infidelity where each axis is the photon occupation number of the spectator mode (x-axis being the 1st spectator, y-axis the 2nd spectator) on a grid representing the cross-Kerr parameters between the target mode and the spectator modes. The title of each subplot represents the cross-Kerr of each oscillator, written in tuples (i, j) where the cross-Kerr to the 1st (2nd) oscillator has cross-Kerr $= 10^{(i-1)/2}\xi$ ($10^{(j-1)/2}\xi$). We see that until the cross-Kerr is very small ($\ll$ the number of photons in a given cavity such that the frequency shift is small relative to the transition frequencies of the target oscillator) we get very high infidelities even for just a few photons in the spectator modes. The infidelities exhibit an oscillatory behavior which roughly correlates with the relative magnitudes of the cross-Kerr parameters of the cavities.

We can simplify the heatmap in Fig. 1 by noting there are a large number of symmetries in the plot. The action on the system Hamiltonian from the spectator modes is conveyed entirely through the term $\varepsilon\hat{V} = -\hat{n}\Sigma_j \xi_j n_j$. Instead of plotting the infidelity as a function of the populations in adjacent modes, we instead plot it against the parameter ε (really, ε/ξ as this is the primary dynamically relevant parameter) in Fig. 2 for each of the four SWAP gates tested. Here we exclude the zero spectator mode photon occupation case (as $\varepsilon = 0$ in that case and thus cannot be placed on a log-log plot). We will simply note that infidelity is $\mathcal{O}(1e-4)$ to $\mathcal{O}(10^{-3})$ in the zero-noise case for each sample. We see that each SWAP gate tested shows the same scaling with ε/ξ for $\varepsilon/\xi \ll 0.001$, scaling with a slope of ≈ 2 on a log-log plot, denoting quadratic scaling in ε, just

SWAP gate	infidelity slope
$\|0\rangle \longleftrightarrow \|3\rangle$	1.95
$\|0\rangle \longleftrightarrow \|4\rangle$	1.98
$\|0\rangle \longleftrightarrow \|5\rangle$	1.94
$\|0\rangle \longleftrightarrow \|6\rangle$	1.84

Table I: Slope in the region of $\varepsilon/\xi = 10^{-4}$ of the infidelity curves to three significant figures for each SWAP gate tested, found by taking the slope of said curve in the region $10^{-4.05} < \varepsilon/\xi < 10^{-3.95}$.

as predicted in Section III.

To make this even clearer, we also plot a rescaling of these infidelities in Fig. 2, with each curve's y-values rescaled such that at a data point for an intermediate value of ε ($\varepsilon = 10^{-4}$) each curve has the same y-axis value. All the data lines up nearly perfectly for more than an order of magnitude from just over 10^{-5} to around $10^{-3.5}$ and only diverges as ε/ξ approaches 0.001. We also provide a table, Table I, showing the slope of the infidelity curves on the log-log plot in the region of 10^{-4}, estimated by taking the slope in the region between $10^{-4.05}$ and $10^{-3.95}$, and all of the slopes are near 2, ie are approximately quadratic.

Thus, we see both from theory and simulation that the effect of spectator modes on the fidelity of a gate generated by a control pulse produced without taking into account spectator modes' frequency shift on the target mode is approximately quadratic in the magnitude of that frequency shift, and rises rapidly to yield an almost orthogonal gate for shifts on the order of 10^{-3} times the qudit nonlinearity.

IV. CONCLUSIONS

We provided a fidelity decay formula and simulated qudit gates in the presence of spectator modes in order to compare the estimated scaling and numerical results. The fidelity formula, Eq. 13, is independent of the gate, so we expect to get a similar scaling for $\varepsilon \to 0$ for gates other than SWAP.

We highlight that these frequency shifts yield extremely stringent bounds on interaction parameters and spectator mode occupations. For future directions, one may try to tackle alleviating the effects of fidelity decay with several useful approaches from quantum computing and error correction, such as dynamical decoupling [19, 22, 23], shortcuts to adiabaticity and steering [24], risk-neutral approaches in robust control [18] and bosonic error correction [25].

ACKNOWLEDGMENT

We thank Jens Koch and Yuri Alexeev for discussions on large-scale simulations. This material is based upon work supported by the U.S. Department of Energy, Office of Science, National Quantum Information Science Research Centers, Superconducting Quantum Materials and Systems Center (SQMS) under contract number DE-AC02-07CH11359. We gratefully acknowledge the computing resources provided on Bebop, a high-performance computing cluster operated by the Laboratory Computing Resource Center at Argonne National Laboratory.

[1] M. Ringbauer, M. Meth, L. Postler, R. Stricker, R. Blatt, P. Schindler, and T. Monz, A universal qudit quantum processor with trapped ions, arXiv preprint arXiv:2109.06903 (2021).
[2] Y. Chi, J. Huang, Z. Zhang, J. Mao, Z. Zhou, X. Chen, C. Zhai, J. Bao, T. Dai, H. Yuan, *et al.*, A programmable qudit-based quantum processor, Nature communications **13**, 1 (2022).
[3] A. Romanenko, R. Pilipenko, S. Zorzetti, D. Frolov, M. Awida, S. Belomestnykh, S. Posen, and A. Grassellino, Three-dimensional superconducting resonators at t< 20 mk with photon lifetimes up to τ= 2 s, Physical Review Applied **13**, 034032 (2020).
[4] X. Wu, S. Tomarken, N. A. Petersson, L. Martinez, Y. J. Rosen, and J. L. DuBois, High-fidelity software-defined quantum logic on a superconducting qudit, Physical Review Letters **125**, 170502 (2020).
[5] M. S. Alam, S. Belomestnykh, N. Bornman, G. Cancelo, Y.-C. Chao, M. Checchin, V. S. Dinh, A. Grassellino, E. J. Gustafson, R. Harnik, *et al.*, Quantum computing hardware for hep algorithms and sensing, arXiv preprint arXiv:2204.08605 (2022).
[6] S. Chakram, K. He, A. V. Dixit, A. E. Oriani, R. K. Naik, N. Leung, H. Kwon, W.-L. Ma, L. Jiang, and D. I. Schuster, Multimode photon blockade, arXiv preprint arXiv:2010.15292 (2020).
[7] S. Chakram, A. E. Oriani, R. K. Naik, A. V. Dixit, K. He, A. Agrawal, H. Kwon, and D. I. Schuster, Seamless high-q microwave cavities for multimode circuit quantum electrodynamics, Physical review letters **127**, 107701 (2021).
[8] Y. Wang, Z. Hu, B. C. Sanders, and S. Kais, Qudits and high-dimensional quantum computing, Frontiers in Physics , 479 (2020).
[9] E. J. Gustafson, Prospects for simulating a qudit-based model of (1+ 1) d scalar qed, Physical Review D **103**, 114505 (2021).
[10] E. Gustafson, Noise improvements in quantum simulations of sqed using qutrits, arXiv preprint arXiv:2201.04546 (2022).

[11] M. Otten, K. Kapoor, A. B. Özgüler, E. T. Holland, J. B. Kowalkowski, Y. Alexeev, and A. L. Lyon, Impacts of noise and structure on quantum information encoded in a quantum memory, Physical Review A **104**, 012605 (2021).

[12] M. S. Blok, V. V. Ramasesh, T. Schuster, K. O'Brien, J.-M. Kreikebaum, D. Dahlen, A. Morvan, B. Yoshida, N. Y. Yao, and I. Siddiqi, Quantum information scrambling on a superconducting qutrit processor, Physical Review X **11**, 021010 (2021).

[13] W.-L. Ma, S. Puri, R. J. Schoelkopf, M. H. Devoret, S. Girvin, and L. Jiang, Quantum control of bosonic modes with superconducting circuits, Science Bulletin **66**, 1789 (2021).

[14] A. Blais, A. L. Grimsmo, S. Girvin, and A. Wallraff, Circuit quantum electrodynamics, Reviews of Modern Physics **93**, 025005 (2021).

[15] C. P. Koch, U. Boscain, T. Calarco, G. Dirr, S. Filipp, S. J. Glaser, R. Kosloff, S. Montangero, T. Schulte-Herbrüggen, D. Sugny, *et al.*, Quantum optimal control in quantum technologies. strategic report on current status, visions and goals for research in europe, arXiv preprint arXiv:2205.12110 (2022).

[16] A. B. Özgüler and D. Venturelli, Numerical gate synthesis for quantum heuristics on bosonic quantum processors, arXiv preprint arXiv:2201.07787 (2022).

[17] N. A. Petersson, F. M. Garcia, A. E. Copeland, Y. L. Rydin, and J. L. DuBois, Discrete adjoints for accurate numerical optimization with application to quantum control, arXiv preprint arXiv:2001.01013 (2020).

[18] N. A. Petersson and F. Garcia, Optimal control of closed quantum systems via b-splines with carrier waves, arXiv preprint arXiv:2106.14310 (2021).

[19] T. Gorin, T. Prosen, T. H. Seligman, and M. Žnidarič, Dynamics of loschmidt echoes and fidelity decay, Physics Reports **435**, 33 (2006).

[20] S.-J. Gu, Fidelity approach to quantum phase transitions, International Journal of Modern Physics B **24**, 4371 (2010).

[21] A. B. Özgüler, C. Xu, and M. G. Vavilov, Response of a quantum disordered spin system to a local periodic drive, Physical Review B **101**, 024204 (2020).

[22] D. A. Lidar, Review of decoherence free subspaces, noiseless subsystems, and dynamical decoupling, arXiv preprint arXiv:1208.5791 (2012).

[23] B. Pokharel and D. A. Lidar, Demonstration of algorithmic quantum speedup (2022).

[24] A. B. Özgüler, R. Joynt, and M. G. Vavilov, Steering random spin systems to speed up the quantum adiabatic algorithm, Physical Review A **98**, 062311 (2018).

[25] W. Cai, Y. Ma, W. Wang, C.-L. Zou, and L. Sun, Bosonic quantum error correction codes in superconducting quantum circuits, Fundamental Research **1**, 50 (2021).